ADVANCED ENGINEERING MATERIALS
www.aem-journal.com

Graphene-Based Magnetocaloric Composites for Energy Conversion

Chiara Coppi, Francesco Cugini, Giacomo Magnani, Chiara Milanese, Lucia Nasi, Laura Lazzarini, Daniele Pontiroli, Mauro Riccò, and Massimo Solzi*

Herein, a simple, versatile, and cost-effective method to fabricate innovative thermal conductive magnetocaloric (MC) composites, which offers a smart solution to manufacture active elements with desired geometries, overcoming the current thermal and mechanical limits of the most studied MC materials, is presented. The composite is prepared by embedding powder of a MC material in an epoxy matrix enriched with a graphene-based material, obtained by thermal exfoliation of graphite oxide. The graphene-enriched composite shows a significant improvement of the MC time response to the magnetic field, due to the formation of a 3D network that bridges the MC particles and reduces the metal–matrix contact resistance, thus creating a percolation path for an efficient heat transfer. Because of the simplicity and scalability of the preparation method and the great enhancement in response time, these new functional composites represent an important step for the effective application of MC materials in thermomagnetic devices for the energy conversion.

1. Introduction

Magnetocaloric (MC) materials are a versatile class of functional materials, in which the complex interactions leading to strong coupling between magnetic and thermodynamic degrees of freedom have opened great opportunities for the development of innovative and eco-friendly energy conversion technologies, such as magnetic refrigeration (MR) or thermomagnetic energy generation.[1,2] The MR is based on the MC effect (MCE), which consists of an entropy change (Δs_T) or a temperature change (ΔT_{ad}) induced in a magnetic material by the variation of an applied magnetic field under isothermal or adiabatic condition.[3] Repeated magnetization and demagnetization processes can be used to design refrigerant cycles, with a gain in terms of energy efficiency and environmental sustainability with respect to common gas-compression refrigerant technologies.[2,3] By exploring the inverse thermomagnetic cycle, thermomagnetic generators (TMGs) convert thermal energy into mechanical or electrical energy. In this way, they offer a chance to recover the low-grade waste heat[2] from sources with temperatures below 100 °C, which represents a large amount of the total industrial and civil waste heat that can be scarcely recovered with available technologies.[4,5] In the past few decades, many prototypes of magnetic refrigerators and TMGs have been developed worldwide.[6,7] Their performance is gradually increasing, as new materials and technologies are discovered. However, these technological innovations still face the same challenge to fully unleash their potential: the search for performant, sustainable, and cost-effective MC materials. Moreover, the field has reached a bottleneck related to a lack of integration of the research focusing on fundamental properties of materials and their technological applications. Bridging the gap between basic properties and engineered functional elements, with optimized performances, is the keystone to boost the mass-market diffusion of MC technologies. Magnetic active elements for MR and TMG should have, besides excellent MC properties, good thermal and mechanical properties.[8,9] Indeed, high-frequency thermomagnetic cycles are needed to increase the efficiency and power of MR and TMG devices, thus requiring a fast heat exchange between the MC active element and a transfer fluid.[2,8] Both the intrinsic thermal conductivity of MC materials and the geometrical configuration of active elements must be optimized to provide the largest heat exchange.[2] Furthermore, the mechanical properties of MC materials must allow the shaping of complex structures and ensure the stability over repeated thermomagnetic cycles. All the most promising classes of MC materials, such as LaFeSi-based compounds, Fe_2P-based compounds, and Heusler alloys, suffer of poor

C. Coppi, F. Cugini, G. Magnani, D. Pontiroli, M. Riccò, M. Solzi
Department of Mathematical, Physical and Computer Sciences
University of Parma
Parco Area delle Scienze 7/A, 43124 Parma, Italy
E-mail: francesco.cugini@unipr.it

C. Coppi, F. Cugini, L. Nasi, L. Lazzarini, M. Solzi
Institute of Materials for Electronics and Magnetism
National Research Council (IMEM-CNR)
Parco Area delle Scienze 37/A, 43124 Parma, Italy

C. Milanese
Pavia Hydrogen Laboratory
C.S.G.I. and Chemistry Department
Physical Chemistry Section
University of Pavia
Viale Taramelli 16, 27100 Pavia, Italy

The ORCID identification number(s) for the author(s) of this article can be found under https://doi.org/10.1002/adem.202200811.

DOI: 10.1002/adem.202200811

mechanical properties and low machinability. Moreover, some of these materials show a degradation of MC properties after device fabrication due to changes in microstructure, composition, or atomic ordering.[10,11] A proposed solution to improve the mechanical stability and the formability of these materials is the use of composites, in which the active MC particles are embedded into a metal or polymer matrix. Different strategies have been tested so far, such as polymer bonded obtained by cold compaction[12–14] and hot pressing with a metallic powder.[15–17] The applicability of the first solution is limited by the drastic reduction of the thermal conductivity of the composite, due to the low thermal properties of the polymeric matrix.[18] In contrast, the metallic matrix promotes the heat transport but represents a large passive thermal mass, absorbing much of the heat generated by the MCE. Moreover, the hot-pressing method likely induces the degradation of MC properties of active material.[15–17]

Here, we present a simple and versatile method to prepare advanced epoxy-based MC composites with improved mechanical and thermal properties promoted by the addition to the epoxy binder of a graphene-based material. The composite is made of polydisperse MC micrometric particles embedded in a polymeric matrix enriched with a small fraction of thermally exfoliated graphite oxide (TEGO).[19–21] Carbon nanostructures, such as graphene, graphene oxide, graphite, and nanotubes, have been recently utilized to improve the thermal conductivity of polymeric resins.[22–25] The use of carbon fillers is also known to enhance mechanical properties in composites,[26,27] making graphene-related materials promising candidates for the preparation of active elements for MRs and TMGs. In our composite, we enrich the epoxy resin with a small amount of TEGO with the aim to design a percolation network that interconnects the conductive MC particles, thus promoting a fast heat exchange. The MC response of the composite was directly measured with a specially designed in-field adiabatic calorimeter on different time scales, demonstrating the positive effect of TEGO in increasing the heat transfer through the composite. The composite enriched with the 0.1 wt% of TEGO shows a complete exploitation of the MCE at a frequency up to 10 Hz, which is the maximum frequency utilized in MR prototypes. The experimental results were combined with 2D finite-element thermal heat exchange simulations, which offer a guideline to further optimize the thermal and MC properties of the composite. The reported results demonstrate the possibility of producing, with a simple and cost-effective procedure, MC composites, also in shape of complex structures or thin plates, with good mechanical and thermal properties.

As the MC test material for the preparation of the composite, we chose a $Ni_2Mn_{1.3}In_{0.7}$ Heusler alloy showing a fully reversible MCE just above room temperature.[28,29] NiMn-based Heusler alloys, with the general formula $Ni_2Mn_{1+x}Z_x$ (with Z an element of the III-V groups or a 3D element), are among the most studied materials for thermomagnetic energy conversion technologies.[8,9] Their flexible lattice allows us to explore a wide range of chemical compositions and to tune their structural, magnetic, and functional properties.[29–32] By varying the composition, both a standard MCE, associated with the ferro-to-paramagnetic transition of the austenitic phase, and a giant MCE, related to the martensitic magneto-structural transition[28,33] can be obtained near room temperature. The high tunability of their MC properties, together with the high thermal conductivity and the absence of rare earths, make these alloys very promising for thermomagnetic applications. However, their poor mechanical properties and the strong dependence of magnetic and MC properties on microstructural features and on the degree of atomic order are drawbacks that currently limit their application in thermomagnetic devices.[10,11,34]

2. Experimental Section

2.1. Preparation of the Composite

The composite was prepared by mixing powder of the NiMnIn Heusler alloy, TEGO, and an epoxy resin, following the step-by-step procedure shown in **Figure 1**. The NiMnIn powder was obtained by manually grinding a bulk sample of $Ni_2Mn_{1.3}In_{0.7}$ synthetized by arc melting (Figure 1b, details are reported in the Supporting Information). The obtained powder was annealed at 773 K for 24 h in argon atmosphere to relax the mechanical stresses introduced during the grinding and restore the magnetic properties of the bulk sample.[10,11,34] The graphene was synthetized via thermal exfoliation of graphite oxide under dynamic vacuum, using a process capable of obtaining a highly defective product (Figure 1a, details are reported in the Supporting Information).[19] These defects were kept active, by avoiding the exposition of as-prepared graphene to the air, and were exploited to promote a grafting effect between the resin matrix and the carbonaceous additive, obtaining a homogeneous dispersion. The epoxy was composed of bisphenol-A epoxy resin-based vinyl ester in styrene (Distitron Ve 100 by Polynt) and a methyl ethyl ketone peroxide (Butanox M-50) used as hardening agent and selected for the low water content and the absence of polar compounds. No metallic accelerator agents had been added to the resin, to avoid possible undesired reactions with MC materials. This resin was selected for the low quantity of air that it incorporates during the mixing. Indeed, the formation of air bubbles inside the polymeric matrix is detrimental to heat transport properties of the composite.

Bulk samples of the composite were prepared by casting the mixture in a Teflon mold. Figure 1d shows, as an example, a hollow cylinder (external diameter of 20 mm, wall thickness of 1 mm, and height of 5 mm) made of the composite, designed to be used as an active element in a "Curie wheel" TMG. Thin plates with a thickness down to 400 μm, showing good mechanical properties (Figure 1e), were obtained by spreading the composite on a Teflon surface. All the samples were then cured at 60 °C for 1 h.

2.2. Characterizations

The morphology of MC powder and composites was studied by a Zeiss Auriga Compact scanning electron microscope (SEM). The high-resolution transmission electron microscopy (HRTEM) and selected area electron diffraction (SAED) analyses were performed by a JEOL 2200FS electron microscope, working at 200 kV, equipped with energy-dispersive spectroscopy (EDS). The samples for transmission electron microscopy (TEM) were prepared by drop casting of the NiMnIn powder suspension on carbon-coated copper grids and by mechano-chemical thinning

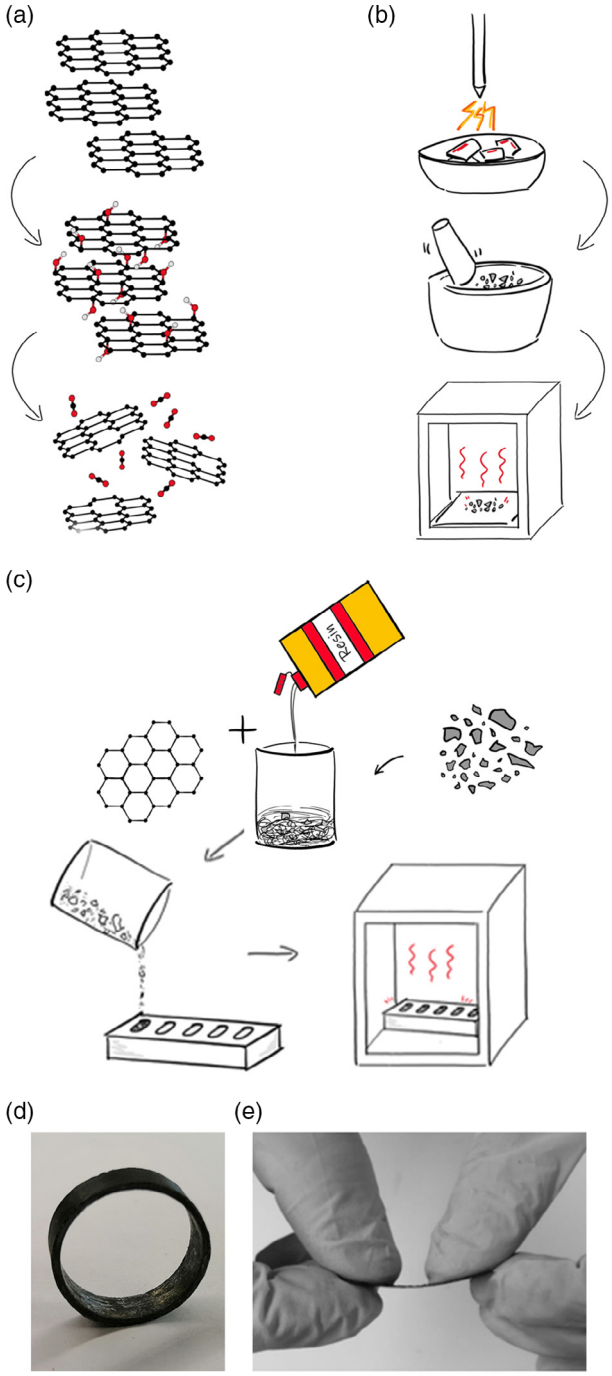

Figure 1. Scheme of the composite preparation route: a) TEGO synthesis; b) preparation of the MC powder (arc-melting synthesis of bulk sample, grinding, and annealing treatment of the powder); c) preparation of the MC composite (mixing, molding, and curing); d) hollow cylinder of MC composite (diameter of 20 mm and wall thickness of 1 mm); and e) thin plate of MC composite with a thickness of 400 µm.

of the bulk composite to about 20 µm followed by Ar ion milling till electron transparency.

The thermal conductivity of the enriched resin and one MC composite at room temperature, prepared as pellets with a diameter of 18 mm and a thickness of 5 mm, was obtained with the modified transient plane source method (conforms to ASTM D7984) by measuring the thermal diffusivity with a TCi Thermal Conductivity Analyzer by C-Therm (Fredericton, New Brunswick, Canada). The specific heat capacity of NiMnIn compound, epoxy resin, and composites was measured, also under an applied magnetic field, through a special designed in-field differential scanning calorimeter, based on thermoelectric elements.[35] The magnetic properties of starting bulk sample, powder, and composites were characterized as a function of temperature and magnetic field with a SQUID magnetometer (MPMS-XL5 by Quantum Design) and an extraction magnetometer (Maglab System2000 by Oxford Instruments). The MCE was directly measured with an adiabatic temperature change probe described in detail in literature.[36] The probe uses a Cernox bare chip temperature sensor (by Lake Shore Cryotronics) to continuously measure the sample temperature. The sensor is characterized by a small thermal mass that ensures a response time of 70 ms. The MCE was induced by a magnetic field variation obtained by turning on/off a low-induction electromagnet (field sweep rate of about 1 T s^{-1}) or by moving, with a pneumatic piston, the probe inside a static magnetic field (field sweep rate of about 10 T s^{-1}). The maximum applied magnetic field was 1.8 T.

3. Results and Discussion

3.1. Morphological Analysis

Combined SEM and HRTEM observations of the MC powder reveal a wide distribution of particle sizes (**Figure 2**a–c). The SEM observations (Figure 2a) show that the grinding process

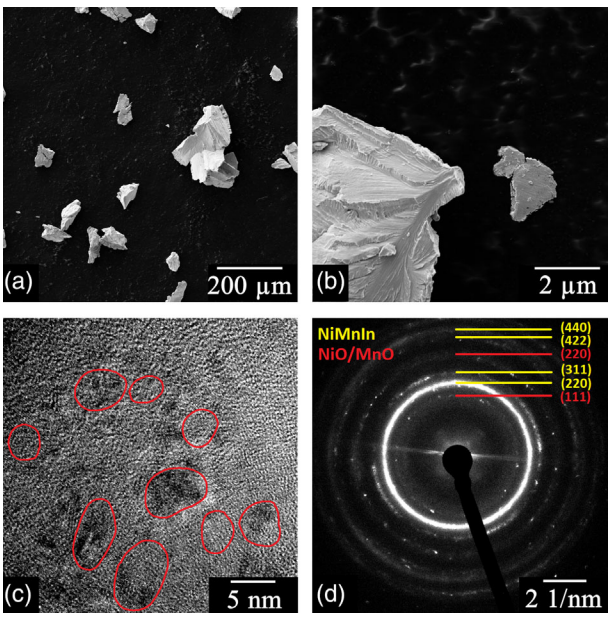

Figure 2. Analysis of the NiMnIn powder: a) SEM image, b) SEM image showing the presence of small particles on the large fragments, c) HRTEM image showing the nanosized particles outlined by the red lines, and d) SAED pattern showing the characteristics rings of NiMnIn and the presence of secondary NiO/MnO phases.

produced fragments with dimensions varying from tens to hundred microns (maximum size about 250 μm). A closer inspection reveals that much smaller particles are present on the larger ones (Figure 2b). The TEM analysis points out the presence of particles as small as 5 nm (**Figure 3**c). The TEM SAED pattern shows rings corresponding to the austenitic phase of NiMnIn (Figure 2d).

The morphology of the composite was analyzed with a multi length-scales approach by combining optical microscopy, SEM, and HRTEM. The optical and SEM observations (Figure 3a,b) reveal a uniform dispersion of the MC powder. No sedimentation effects or holes caused by air bubbles are evident. The dark contrast visible in the SEM image of Figure 3b is due to grains of MC powder that were detached during the lapping of the sample surface. TEM observations were done on a mechanically thinned layer of composite to investigate the TEGO distribution at the nanoscale. The mechano-chemical thinning process has been an especially hard task, due to surprising mechanical properties of the prepared composite material. The HRTEM analysis (Figure 3c) shows the presence of randomly oriented nanometric MC particles dispersed into the matrix, as evidenced by the rings in the SAED pattern reported in Figure 3d. Here, the same rings as in the starting powder diffraction pattern are present, together with a broad ring at 0.34 nm, consistent with the stacking distance of carbon sheets in TEGO. The EDS performed in the TEM does not reveal the formation of TEGO clusters, suggesting a uniform distribution of TEGO in the polymeric matrix. The combination of microscopic observations at different length scales returns a morphology of the composite characterized by a homogeneous dispersion of MC particles, with dimensions ranging from nanometers to tens of micrometers, into the uniform epoxy–graphene matrix.

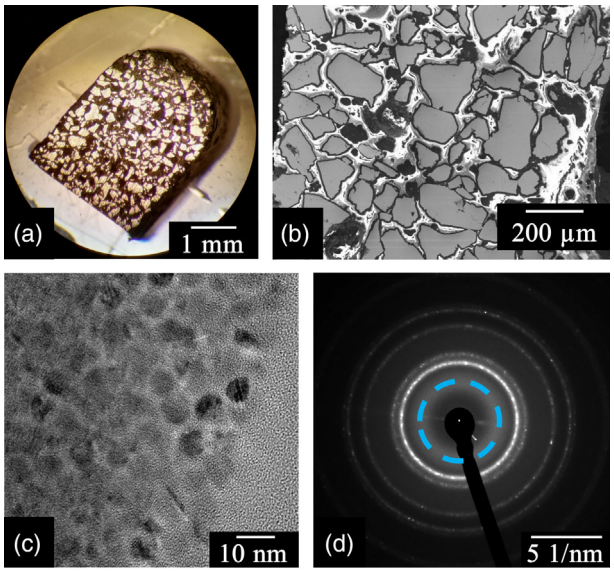

Figure 3. Morphology of MC composite with TEGO at different length scales: a) optical microscopy image, b) SEM image, c) HRTEM image, and d) SAED pattern showing the rings related to the NiMnIn together with the ring corresponding to the stacking distance of TEGO (the blue dotted line).

The broad size distribution of MC particles allows us to obtain composites with a huge amount of MC powder (up to the 88% of weight concentration), favoring the increase in exploitable MCE. Indeed, finite-element heat transfer simulations of the system (details are reported in Supporting Information) demonstrate that both the adiabatic temperature change and the characteristic time of heat transfer scale with the concentration of MC powder in the composite (Figure S2, Supporting Information). For example, fixing the particle sizes, the calculated adiabatic temperature change ΔT_{ad} can increase about 50% from low (60%) to high (84%) MC weight concentration and the characteristic time of heat exchange is reduced by a factor of 2. This twofold benefit is enhanced considering a more conductive matrix due to the addition of TEGO to the resin.

3.2. Thermal Properties

Thermal conductivity and heat capacity measurements of the composite revealed an increase in thermal diffusivity of the resin due to the TEGO addition. Thermal conductivity analysis has been performed on the epoxy matrix enriched with TEGO in different weight concentrations, from 0 to 0.5 wt% (Figure S5, Supporting Information). The highest thermal conductivity λ is reached with an intermediate TEGO concentration of about 0.1 wt%: the addition of TEGO increases the thermal conductivity of the resin by 28% (from 0.18 to 0.23 $W\,m^{-1}\,K^{-1}$). At higher concentration, the TEGO tends to agglomerate into the matrix, thus avoiding the further improvement of thermal conductivity. Together with the increase in the thermal conductivity with 0.1 wt% TEGO enrichment, we observed a 17% decrease in the specific heat c_p (from 1100 to 915 $J\,kg^{-1}\,K^{-1}$, Supporting Information). In this way, a total 56% gain of thermal diffusivity ($\alpha = \lambda/\rho\ c_p$, where ρ is the density) was obtained.

The thermal conductivity of the composite further increases by adding the MC powder with the TEGO-enriched resin. A composite made of 80 wt% of MC powder and the resin enriched with 0.1 wt% of TEGO showed a thermal conductivity of 1.03 $W\,m^{-1}\,K^{-1}$.

3.3. Magnetic and MC Properties

The magnetic and MC properties of the composites, with and without TEGO, were investigated and compared with the ones of starting Heusler sample. In **Figure 4**, we report the magnetization as a function of temperature measured around the Curie transition at 1 T for the composites at 80 wt% (MC80) and 88 wt% (MC88) of MC powder. The mass magnetization is reduced in the composite proportionally to the weight concentration of the polymeric matrix, whereas the Curie transition is not modified by the composite preparation procedure. The normalized $M(T)$ temperature behavior of composites overlaps with that of starting Heusler sample (inset of Figure 4), thus demonstrating that the performed annealing treatment of Heusler powder is enough to fully recover the magnetic properties of the starting bulk compound.

The reduction of mass magnetization, due to the dilution of the magnetic material with the nonmagnetic resin, proportionally affects the isothermal entropy variation of the composites

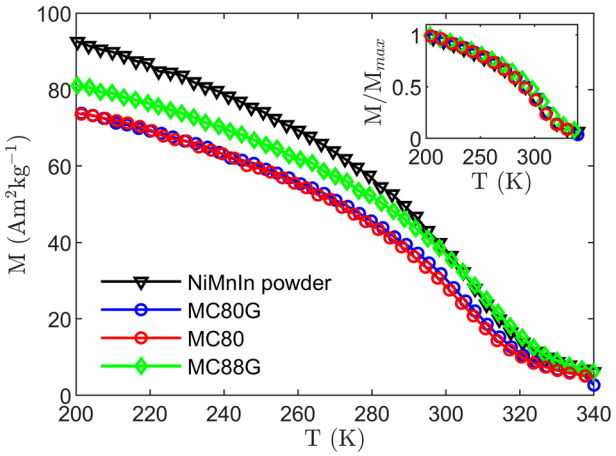

Figure 4. Temperature dependence of magnetization measured under a magnetic field of 1 T of NiMnIn annealed powder, composites at 80 and 88 wt% MC with (MC80G, MC88G) or without (MC80) TEGO (at 0.1 wt%). Inset: temperature dependence of magnetization normalized to the maximum value.

(Δs_T). **Figure 5**a shows the Δs_T, for a magnetic field change of 1.8 T, obtained by applying the Maxwell equation to $M(T)$ data collected at different applied magnetic fields.[36] All the composites, with and without TEGO, display a maximum of Δs_T at the same temperature of the starting bulk alloy (306 ± 1 K). The Δs_T rescales proportionally to the weight concentration of the active MC powder. Both the composites with 80 wt% powder, with and without TEGO (MC80G and MC80), have a maximum Δs_T of (2.1 ± 0.1) J kg^{-1} K^{-1}, which corresponds to (78 ± 6)% of the maximum Δs_T of the bulk NiMnIn sample. Increasing the powder concentration to 88 wt% (MC88G), the Δs_T reaches 2.3 ± 0.1 J kg^{-1} K^{-1}, which is (85 ± 6)% of the maximum Δs_T of the starting sample.

The MC characterization was obtained also directly through a special designed adiabatic calorimeter that measures the adiabatic temperature change induced in the material by the application of a magnetic field. Figure 5b shows the temperature dependence of the ΔT_{ad}, induced by a magnetic field variation of 1.8 T, for the composite with (MC80G, MC88G) and without (MC80) TEGO, compared with the one of bulk NiMnIn sample. The maximum $\Delta T_{ad,C}$ of the composites decreases with respect to that of bulk compound $\Delta T_{ad,B}$, following Equation (1), which takes into account the specific heat capacity c_p and the percentage weight concentration wt% of MC ($c_{p,MC}$, wt%$_{MC}$) and matrix ($c_{p,MATR}$, wt%$_{MATR}$) component

$$\Delta T_{ad,C} = \Delta T_{ad,B} \cdot \frac{c_{p,MC} \cdot \text{wt\%}_{MC}}{c_{p,MC} \cdot \text{wt\%}_{MC} + c_{p,MATR} \cdot \text{wt\%}_{MATR}} \quad (1)$$

This reduction is caused by the thermal mass of the matrix that absorbs part of the heat induced by the MCE. The ΔT_{ad} rescales, as in the case of Δs_T, with the percentage weight concentration of MC material. Moreover, comparing the composites with and without TEGO, we observed a higher value of ΔT_{ad} in the TEGO-enriched composite, thanks to the lower specific heat of the matrix. Although both values of ΔT_{ad} are lower than those theoretically calculated from Equation (1), the adiabatic temperature change of the composite with graphene is closer to the predicted value than the one of the samples without TEGO. This suggests that TEGO reduces the heat dissipation effects, promoting the heat flux from the MC particles toward the temperature sensor.

The time dependence of the MC response of composites has been investigated by directly measuring the adiabatic temperature change induced in the samples by using different magnetic field variation rates.[18,37,38] **Figure 6** shows the time evolution of the adiabatic temperature change of the bulk NiMnIn compound and the composites. The two panels report the dynamic MC response of samples in two different time scales. Figure 6a shows the temperature change induced by a field variation of 1.8 T in 1 s (magnetic field sweep rate of 1.8 T s^{-1}), whereas the measurements reported in Figure 6b were collected with a magnetic field variation of about 18 T s^{-1}. At the lower field rate, all the measurements are superimposed, and the temperature change of all samples follows the magnetic field variation (Figure 6a). This result agrees with finite-element simulations of heat transfer in the composites that predicted a characteristic time for heat exchange of a few tens of milliseconds (Figure S2–S4, Supporting Information).

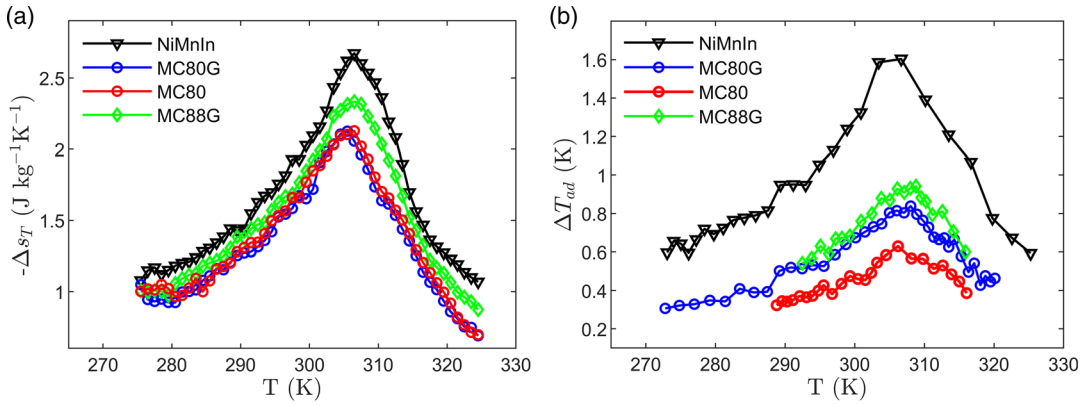

Figure 5. a) Isothermal entropy change and b) adiabatic temperature change as a function of temperature in a magnetic field variation of 1.8 T of NiMnIn bulk sample, the composites at 80 and 88 wt% MC with (MC80G, MC88G) or without (MC80) TEGO.

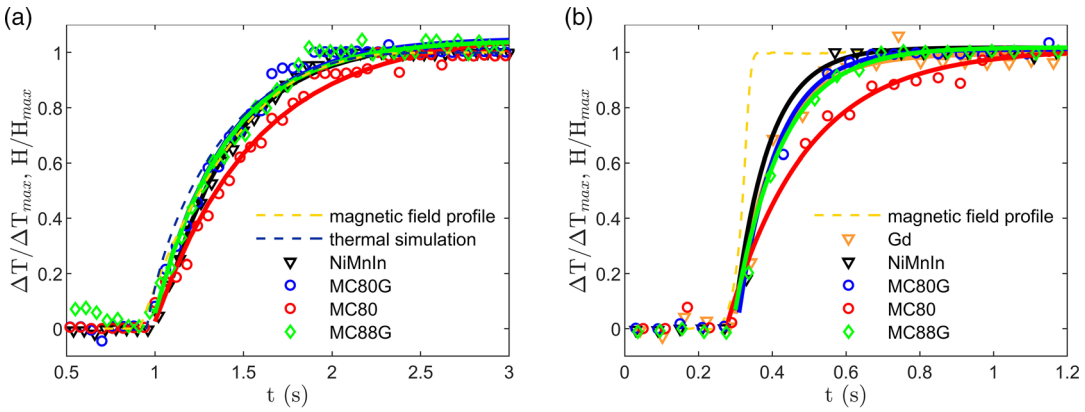

Figure 6. Time evolution of MC response to slow a) or fast b) magnetic field variation of NiMnIn, Gd, and composites with (MC80G, MC88G) and without (MC80) TEGO. The adiabatic temperature change is normalized to the maximum value. The solid lines correspond to exponential fits of the experimental data. Yellow dashed curves are the magnetic field profiles for the two experimental setups. (a) Dark blue line is the simulated MC composite + TEGO response.

Instead, when the rate of field variation increases to 18 T s^{-1}, the response of the composite without TEGO (MC80) shows a clear delay as compared with the starting Heusler sample and the TEGO-enriched composite. Both TEGO-enriched composites at 80 and 88 wt% show a characteristic time of the temperature variation τ of 0.10 ± 0.03 s, which is the same time response of the starting Heusler sample (which has a thermal conductivity $\lambda = 19.0\ W\ m^{-1}\ K^{-1}$[8]) and a benchmark Gd bulk sample ($\lambda = 7.5\ W\ m^{-1}\ K^{-1}$[8]). The constant delay with respect to the field variation, observable for all samples, is due to the characteristic time of the temperature sensor, as described in detail in literature.[18,37,38] In contrast, the adiabatic temperature change for the composite without TEGO is characterized by a response time to the magnetic field about two times larger ($\tau = 0.21 \pm 0.03$ s) as compared with the composite with TEGO. The same delay has been reported also for epoxy-bonded composites of LaFeSi ($\tau = 0.22$ s[38]) and MnfePSi ($\tau = 0.20$ s[18]) compounds. These results clearly demonstrate that TEGO improves the heat transport in the composite, thus recovering the in-time MC response of the bulk metallic compound and preventing the effect of low thermal conductivity of the polymeric resin.

It is worth noting that the heat transfer simulations of the composite, performed considering the measured thermal properties of the resin (details are reported in Supporting Information), do not justify the observed time delay in the MC response of the composite without TEGO. Indeed, it has already been demonstrated that the main cause of the worsening of heat transport in a composite made of metallic powder and an epoxy binder matrix is the interfacial thermal resistance at the powder–matrix interface, which is not considered in the simulated model.[38]

The relevant effect of TEGO addition on the transport of heat induced by the MCE can be explained by considering an effective decrease in the thermal resistance at the powder–matrix interface and the creation of a percolation network that provides a low thermal resistance path for phonon transport. These beneficial effects have been already observed in heat-conductive composite materials enriched with carbon nanostructures.[39–41] The formation of a 3D network of TEGO[42] anchored to the MC particles is promoted by the high density of active defects, that fosters its homogeneous dispersion and the adhesion to metallic particles. This network provides a preferential low-resistance path for the escape of heat produced by the MCE in the particles. Instead, the overall thermal conductivity of the TEGO-enriched composite does not significantly increase respect to the one of pure resin due to the formation of multiple in-series high- and low-conductive paths made of TEGO + MC powder and resin. The combination of an high-conductive path for MC heat escape and a medium thermal conductivity of the bulk material is favorable for the establishment of a large thermal gradient in active magnetic regenerators for MR.[2]

4. Conclusion

In conclusion, we have presented a simple, cost-effective, versatile, and scalable method to prepare epoxy-based MC composites showing improved thermal diffusivity, a high formability, and good mechanical properties. The composite is produced by embedding powder of an MC material in an epoxy binder matrix enriched with a graphene-based material, obtained by thermal exfoliation of graphite oxide. The active defects of TEGO promote its homogeneous dispersion and adhesion to metallic particles. The thermal characterization of the enriched resin and the dynamic measurement of the MCE over different time scales clearly demonstrated the twofold effect of TEGO in increasing the thermal diffusivity of the binder matrix and decreasing the thermal resistance at the MC particle–epoxy matrix interface. The combination of these two effects promotes the heat transfer in the MC composite and allows us to obtain a fast MC response with a characteristic time twice lower than that of the composite without TEGO. The proposed method can be easily utilized to produce composites starting from powder of all MC materials that can be shaped in on-demand structures by using standard casting techniques. This offers a new perspective and an opportunity to overcome the mechanical and thermal

drawbacks faced in the preparation of active elements for magnetic refrigerators and TMGs.

Further improvements of thermal and MC properties of the composite can be obtained through an increase in the percentage of active magnetic material by using the efficient dispersion methods, such as sonication, roll milling, or high share mixing. Moreover, thermal properties of the matrix can be optimized by designing special 3D graphene structures through specific preparation routes, as reported in literature for thermal-conductive composites.[42]

Supporting Information

Supporting Information is available from the Wiley Online Library or from the author.

Acknowledgements

F.C. acknowledges E. Bruck and the FAME group at TU Delft (Netherlands) for support in the preparation and characterization of the MC bulk sample.

Open Access Funding provided by Universita degli Studi di Parma within the CRUI-CARE Agreement.

Conflict of Interest

The authors declare no conflict of interest.

Data Availability Statement

The data that support the findings of this study are available from the corresponding author upon reasonable request.

Keywords

composites, energy conversion, graphene, Heusler compounds, magnetic refrigeration, magnetocaloric materials, thermally exfoliated graphite oxide

Received: June 7, 2022
Revised: September 7, 2022
Published online: October 6, 2022

[1] X. Moya, N. D. Mathur, *Science* **2020**, *370*, 797.
[2] A. Kitanovski, *Adv. Energy Mater.* **2020**, *10*, 1903741.
[3] V. Franco, J. S. Blázquez, J. J. Ipus, J. Y. Law, L. M. Moreno-Ramírez, A. Conde, *Prog. Mater. Sci.* **2018**, *93*, 112.
[4] C. Forman, I. K. Muritala, R. Pardemann, B. Meyer, *Renewable Sustainable Energy Rev.* **2016**, *57*, 1568.
[5] H. Jouhara, N. Khordehgah, S. Almahmoud, B. Delpech, A. Chauhan, S. A. Tassou, *Therm. Sci. Eng. Prog.* **2018**, *6*, 268.
[6] A. Greco, C. Aprea, A. Maiorino, C. Masselli, *Int. J. Refrig.* **2019**, *106*, 66.
[7] R. A. Kishore, S. Priya, *Renewable Sustainable Energy Rev.* **2018**, *81*, 33.
[8] T. Gottschall, K. P. Skokov, M. Fries, A. Taubel, I. Radulov, F. Scheibel, D. Benke, S. Riegg, O. Gutfleisch, *Adv. Energy Mater.* **2019**, *34*, 1901322.
[9] D. Dzekan, A. Waske, K. Nielsch, S. Fähler, *APL Mater.* **2021**, *9*, 011105.
[10] F. Cugini, L. Righi, L. Van Eijck, E. Brück, M. Solzi, *J. Alloys Compd.* **2018**, *749*, 211.
[11] G. Cavazzini, F. Cugini, F. Puglielli, S. Fabbrici, D. Delmonte, G. Trevisi, L. Nasi, L. Righi, S. Ener, L. Pfeuffer, D. Koch, O. Gutfleisch, F. Albertini, M. Solzi, *J. Alloys Compd.* **2022**, *906*, 164377
[12] C. R. H. Bahl, K. Navickaitė, H. Neves Bez, T. Lei, K. Engelbrecht, R. Bjørk, K. Li, Z. Li, J. Shen, W. Dai, J. Jia, Y. Wu, Y. Long, F. Hu, B. Shen, *Int. J. Refrig.* **2017**, *76*, 245.
[13] H. Zhang, Y. Sun, Y. Li, Y. Wu, Y. Long, J. Shen, F. Hu, J. Sun, B. Shen, *J. Appl. Phys.* **2015**, *117*, 063902.
[14] B. Pulko, J. Tušek, J. D. Moore, B. Weise, K. Skokov, O. Mityashkin, A. Kitanovski, C. Favero, P. Fajfar, O. Gutfleisch, A. Waske, A. Poredoš, *J. Magn. Magn. Mater.* **2015**, *375*, 65.
[15] M. Zhang, Y. Ouyang, Y. Zhang, J. Liu, *J. Alloys Compd.* **2020**, *823*, 153846.
[16] I. A. Radulov, D. Y. Karpenkov, K. P. Skokov, A. Y. Karpenkov, T. Braun, *Acta Mater.* **2017**, *127*, 389.
[17] J. Liu, M. X. Zhang, Y. Y. Shao, A. R. Yan, *IEEE Trans. Magn.* **2015**, *51*, 18.
[18] G. Porcari, K. Morrison, F. Cugini, J. A. A. Turcaud, F. Guillou, A. Berenov, N. H. H. Van Dijk, E. H. H. Brück, L. F. F. Cohen, M. Solzi, *Int. J. Refrig.* **2015**, *59*, 29.
[19] M. Gaboardi, R. Tatti, G. Bertoni, G. Magnani, R. Della Pergola, L. Aversa, R. Verucchi, D. Pontiroli, M. Riccò, *Surf. Sci.* **2020**, *691*, 121499.
[20] M. Gaboardi, A. Bliersbach, G. Bertoni, M. Aramini, G. Vlahopoulou, D. Pontiroli, P. Mauron, G. Magnani, G. Salviati, A. Züttel, M. Riccò, *J. Mater. Chem. A*,**2014**, *2*, 1039.
[21] M. Riccò, D. Pontiroli, M. Mazzani, M. Choucair, J. A. Stride, O. V. Yazyev, *Nano Lett.*,**2011**, *11*, 4919.
[22] A. A. Balandin, S. Ghosh, W. Bao, I. Calizo, D. Teweldebrhan, F. Miao, C. Ning Lau, *Nano Letters* **2008**, *8*, 902.
[23] Y. J. Wan, L. C. Tang, L. Gong, D. Yan, Y. Li, L. Wu, J. Jiang, G. Q. Lai, *Carbon* **2014**, *69*, 467.
[24] W. Guo, G. Chen, *J. Appl. Polym. Sci.* **2014**, *131*, 40565.
[25] S. H. Song, K. H. Park, B. H. Kim, Y. W. Choi, G. H. Jun, D. J. Lee, B. S. Kong, K. W. Paik, S. Jeon, *Adv. Mater.* **2013**, *25*, 732.
[26] L. C. Tang, Y. J. Wan, D. Yan, Y. B. Pei, L. Zhao, Y. Li, L. Wu, J. X. Jiang, G. Q. Lai, *Carbon*,**2013**, *60*, 16.
[27] [M. A. Rafiee, J. Rafiee, Z. Wang, H. Song, Z. Z. Yu, N. Koratkar. *ACS Nano* **2009**, *3*, 3884.
[28] S. Singh, L. Caron, S. W. D'Souza, T. Fichtner, G. Porcari, S. Fabbrici, C. Shekhar, S. Chadov, M. Solzi, C. Felser, *Adv. Mater.* **2016**, *28*, 3321.
[29] G. Cavazzini, F. Cugini, M. E. Gruner, C. Bennati, L. Righi, S. Fabbrici, F. Albertini, M. Solzi, *Scr. Mater.* **2019**, *170*, 48.
[30] F. Cugini, S. Chicco, F. Orlandi, G. Allodi, P. Bonfà, V. Vezzoni, O. N. Miroshkina, M. E. Gruner, L. Righi, S. Fabbrici, F. Albertini, R. De Renzi, M. Solzi, *Phys. Rev. B* **2022**, *105*, 174434.
[31] S. Fabbrici, F. Cugini, F. Orlandi, N. Sarzi Amadè, F. Casoli, D. Calestani, R. Cabassi, G. Cavazzini, L. Righi, M. Solzi, *J. Alloys Compd.* **2022**, *899*, 163249.
[32] S. Fabbrici, G. Porcari, F. Cugini, M. Solzi, J. Kamarad, Z. Arnoldd, R. Cabassi, F. Albertini, *Entropy* **2014**, *16*, 2204.
[33] J. Liu, T. Gottschall, K. Skokov, J. D. Moore, O. Gutfleisch, *Nat. Mater.* **2012**, *11*, 620.
[34] G. Cavazzini, F. Cugini, D. Delmonte, G. Trevisi, L. Nasi, S. Ener, D. Koch, L. Righi, M. Solzi, O. Gutfleisch, F. Albertini, *J. Alloys Compd.* **2021**, *872*, 159747.

[35] G. Porcari, F. Cugini, S. Fabbrici, C. Pernechele, F. Albertini, M. Buzzi, M. Mangia, and M. Solzi, *Phys. Rev. B Condens. Matter Mater. Phys.* **2012**, *86*, 104432.
[36] G. Porcari, M. Buzzi, F. Cugini, R. Pellicelli, C. Pernechele, L. Caron, E. Brück, M. Solzi, *Rev. Sci. Instrum.* **2013**, *84*, 073907.
[37] F. Cugini, M. Solzi, *J. Appl. Phys.* **2020**, *127*, 123901.
[38] K. Sellschopp, B. Weise, M. Krautz, F. Cugini, M. Solzi, L. Helmich, A. Waske, A. Hütten, A. Waske, *Energy Technol.* **2018**, *6*, 1448.
[39] M. Shtein, R. Nadiv, M. Buzaglo, K. Kahil, O. Regev, *Chem. Mater.* **2015**, *27*, 2100.
[40] X. Shen, Z. Wang, Y. Wu, X. Liu, Y. B. He, J. K. Kim, *Nano Lett.* **2016**, *16*, 3585.
[41] Z. Barani, A. Mohammadzdeh, A. Geremew, C. Y. Huang, D. Coleman, L. Mangolini, F. Kargar, A. A. Balandin, *Adv. Funct. Mater.* **2020**, *30*, 1904008.
[42] G. Lian, C. C. Tuan, L. Li, S. Jiao, Q. Wang, K. S. Moon, D. Cui, C. P. Wong, *Chem. Mater.* **2016**, *28*, 6096.